RSC Advances

ROYAL SOCIETY OF CHEMISTRY

www.rsc.org/advances

Journal Name

Dynamic Article Links►

Cite this: DOI: 10.1039/coxxoooooox

www.rsc.org/xxxxxx

ARTICLE TYPE

MnO_2 Doped Polyaniline Grafted Rice Husk Ash Nanocomposites and their Electrochemical Capacitor Applications

P. Prabunathan[a], K. Sethuraman[a] and M. Alagar[a]*

Received (in XXX, XXX) XthXXXXXXXXX 20XX, Accepted Xth XXXXXXXXX 20XX

DOI: 10.1039/b000000x

*[a] Polymer Composite Lab, Department of Chemical Engineering, Anna University, Chennai, 600 025, Tamilnadu, India. *E-mail: mkalagar@yahoo.com Fax: +91 4422359164; Tel: +91 4422359164.*

The utilization of renewable rice husk ash (RHA) for an energy storage system without any activation is described. Polyaniline grafted RHA (PANI/RHA) and MnO_2 doped polyaniline grafted RHA (PANI/MnO_2/RHA) nanocomposites were developed. The capacitance behaviour of the developed nanocomposites was well studied using cyclic voltammetry and charging-discharging methods. The results of galvanostatic charging and discharging show that 17 fold improvement on capacitance behaviour of PANI/RHA and 54 fold enhanced capacitance of PANI/MnO_2/RHA nanocomposites than that of neat RHA. The enhanced capacitance and rate capability of RHA are attributed to the synergistic effect of polyaniline with RHA and also high utilization of pseudo active species for the ion/electron transfer.

Introduction

In recent years, natural environment is gradually endangered by the diversity of hazardous materials released from man-made products and wastes of biomass sources.[1] Similarly, increasing demands over fossil fuel energy and an increasing awareness of sustainability issues made to utilize justifiable biomass for the energy generation as well as storage applications, which helps to reduce the use of environmental hazardous materials.[2] The carbon, carbon based composites with conductive polymers (polyaniline, polypyrrole) and pseudo capacitive materials (RuO_2, MnO_2 and CeO_2), are well known super capacitor anode materials. Their synergistic effects towards the capacitor performance are also well described. [3–8] The activated carbon from bio-sources is reported in the direction of proper usage of renewable materials towards storage applications. However, the synthetic methods of activated carbon involves less economical multistep pathways and utilize activating agents ($ZnCl_2$, H_3PO_3, etc). [9-12]

One of the major naturally occurring bio resource is rice husk ash (RHA) and the most prolific agricultural residue from agriculture based countries, which has been utilized in the wide range of applications in different forms. The major constituents of rice husk were silica (SiO_2) about 60% and carbon (C) ranging from 10 to 40 %. It is also reported that the silica derived from rice husk ash (RHA) was used as a catalyst support, [13] adsorbent, [14] and composites. [15] Similarly, it was reported that RHA was used as an electrode material and electrical capacitors. [16-18] Thus, the crystalline nanosized silicon derived from the rice husk ash has been used as a promising anode materials for Li ion batteries [19, 20] and the activated carbon from rice husk ash also utilized as a capacitor anode materials [21, 22]. Rice husk constitutes of silica exhibiting an insulating behavior and a carbonaceous material contributes for the conductive behavior. Thus, the insulating behavior of RHA will be exploited by compositing the materials with conducting substrates and can be used for the energy storage systems. Likewise, it has been reported that the use of silica core offers high colloidal stability and easily controllable particle size [2].

The present work limelight's the performance of naturally available RHA bio source towards the fabrication of super capacitor anode materials. Similarly, the sustainable RHA was composited with MnO_2 doping and polyaniline grafting without activation process. Grafting of polyaniline over the RHA was primarily ascertained with FT-IR and CP-MAS. Further the doping of MnO_2 on the RHA was supported by XPS and analytical characterization methods such as HR-SEM/EDAX and HR-TEM analysis. Electrochemical studies of PANI/RHA and PANI/MnO_2/RHA composites suggest that the developed nanocomposites are highly suitable towards the fabrication of supercapacitor anodes without utilizing any activation process.

Experimental Section

Materials

Manganese sulphate (≥99.8%) obtained from Alfa aesar). Aniline (monomer), ammonium per sulphate, potassium permanganate, sodium sulfate and hydrochloric acid were obtained from Merck, India and double distilled water was used throughout the work.

Step 1 Synthesis of rice husk ash (RHA)

The rice husk was collected from the local agriculture wasting place and it was synthesized as per the previously reported procedure. [23] Initially, rice husk was washed with distilled water and dried in hot air oven at approximately 60 °C for 8 h. Then washed with acetone, followed by HCl (0.3 M) to remove other contaminants and subsequently dried in hot air oven at approximately 60 °C for 8 h. Finally, rice husk was placed in the muffle furnace for 6 h at

350 °C in order to obtain pure rice husk ash (RHA). The compositions of the resulted products are given in the supporting information (Figure S1b and Table S3). For comparison, the composition of raw rice husk ash is also given (Figure S1a, supporting information).

Step 2 Synthesis of polyaniline grafted rice husk ash (PANI/RHA)

The grafting of highly conductive polyaniline over rice husk ash (PANI/RHA) was developed as per the reported procedure.[24] 1 g of rice husk ash and 1 mL of freshly distilled aniline monomer were added to the 50 mL of 1 M HCl and subsequently sonicated for 30 minutes. Then, the required amount of homogeneous solution containing ammonium per sulphate dissolved in 50 mL of hydrochloric acid (1 M) was slowly added with simultaneous efficient agitation for 5 h at 0-5°C in an ice bath. Then, the expected product was filtered, subsequently washed with 1 M HCl for several times and finally using deionized water to separate the impurities. The resulting product then dried at 60 °C in hot air oven for 12 h.

Step 3 Synthesis of polyaniline grafted MnO_2 doped rice husk ash PANI/MnO_2/RHA nanocomposites.

RHA prepared in the previous step 1 was dispersed in acidified water (pH=2), then desired amount of $MnSO_4.H_2O$ (0.1M) was added and subjected to ultra-sonication for 1 h. Later equivalent amount of $KMnO_4$ (0.05M) dissolved in water (pH=2) was added slowly under continuous sonication for 3 h. Subsequent stirring of the mixture for overnight yields MnO_2 doped RHA (MnO_2/RHA). The resulted product was centrifuged with repeated washing. After drying the same was utilized to graft polyaniline with repeating the above mentioned procedure (step 2).

Characterization

FT-IR spectra data were obtained from Perkin Elmer 6X FT-IR spectrometer. The solid state NMR of raw RHA and RHA/polyaniline were analyzed at 14.1 and 11.7 T respectively on a Bruker DRX-500 spectrometer, equipped with 4 mm MAS probes. Thermo gravimetric analysis (TGA) was performed on a Netzsch STA 409 thermo gravimetric analyzer. A Hitachi S-4800 High resolution - Scanning Electron Microscope (HR-SEM) equipped with Horiba was used to record the morphology with their composition at 20 kV. HRTEM images were captured using TECNAI G_2 S-Twin transmission electron microscope, with an acceleration voltage of 150 kV. TEM samples were prepared by dispersing the composites in ethanol and mounted on carbon-coated Cu TEM grids and dried for 24 h at 30 ^oC to obtain a film of <100 nm in size. Powder X-ray diffraction patterns (XRD) was recorded using a Rigaku Miniflex diffractometer

with Cu-KR radiation (k = 0.154 nm). The diffraction data was recorded in the 2θ over the range of 5–80°. The XPS was measured using an Omicron nanotechnology instrument at a pressure below 10^{-10} Torr. The wide scan was used to recorded core level of atoms with a monochromatic Al-Ka radiation (photon energy ¼ 1486.6 eV) at a pass energy of 15 V and electron take-off angle of 608°.

The electrochemical measurements were carried out in CHI660D electrochemical workstation. Three-electrode assembly was equipped with a working electrode, a platinum counter electrode and Ag/AgCl reference electrode. In the present work fabrication of working electrode was achieved by coating a paste of nanocomposites into a pre cleaned nickel plate with surface area of $1cm^2$. Without adding any carbon, 2 mg of the prepared nanocomposites were mixed with few drops of DMF, coated over the plate and subsequently allowed to dry overnight at 90 °C. Thus the obtained electrode was utilized as a working electrode. Sodium sulphate (0.5 M) was used as an electrolyte to analyze the performance of working electrode. Cyclic voltammetry (CV), galvanostatic charge – discharge measurements and electrochemical impedance analysis were used to study the capacitance behavior of the nanocomposites. The specific capacitance of the nanocomposites was calculated from the discharge curve using the following formula:

$$C = \frac{I \times t}{m \times \Delta V} \qquad (1)$$

Results and Discussion

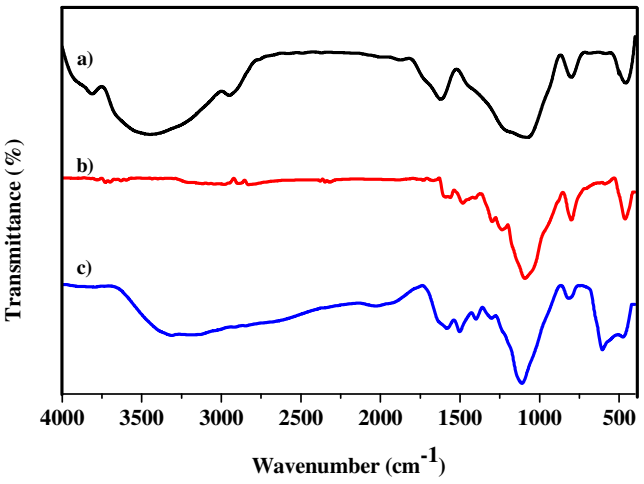

Figure 1. FTIR spectra of a) RHA b) PANI/RHA and c) PANI/MnO_2/RHA nanocomposites.

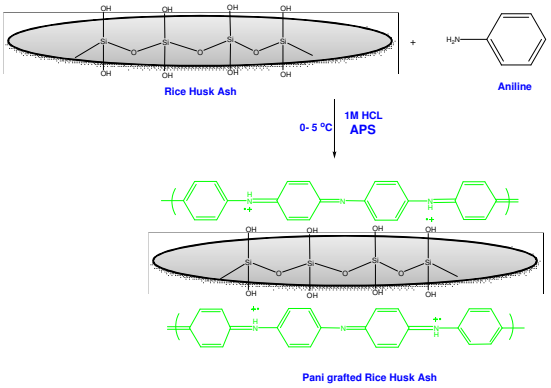

Scheme 1. Synthesis of polyaniline grafted rice husk ash nanocomposite.

FT-IR spectra of RHA, PANI/RHA and PANI/MnO_2/RHA nanocomposites are presented in Figure 1a-c. In Figure 1a, the peaks at 1098, 799 and 465 cm^{-1} was due to Si-O-Si and Si-H vibrations of RHAs amorphous silica. The peak appeared at 2924 cm^{-1} corresponds to the C-H group. The broad peak around 3450 cm^{-1} corresponds to the presence of hydroxyl group in

both water and Si-OH. The grafting of polyaniline over rice husk ash is illustrated in **scheme 1** and their corresponding vibrational spectrum is shown in Figure 1b. The peaks at 1570 and 1476 cm^{-1} corresponds to the typical C=C stretching vibration of the quinoid and benzenoid rings of polyaniline, whereas the peak at 1302 cm^{-1} is attributed to C–N stretching vibration. [24-27] Similar stretching modes were also observed in the Figure 1c with an additional peak at 542 cm^{-1} representing the presence of MnO_2 in the nanocomposites and are in consistent with previously reported literature. [28]

The ^{13}C CP-MAS spectra of RHA and PANI/RHA are shown in Figure 2a and 2b, respectively. The ^{13}C NMR signal at 29 ppm is may be due to the presence of lignin or cellulose carbon, whereas the peak at 128 and 132 ppm corresponds to the aromatic carbon of cellulose. The ^{13}C NMR of PANI/RHA (Figure 2b) was used to illustrates the presence of benzoid and quinoid aromatic carbon of polyaniline, at 124.34 and 144.27 ppm respectively. Further the silica network of RHA and PANI/RHA was confirmed by ^{29}Si CP-MAS spectra, as shown in Figure 2c and 2d respectively. The RHA exhibits three well defined characteristic peaks such as -91, -99 and -109 ppm, which indicates that the presence of

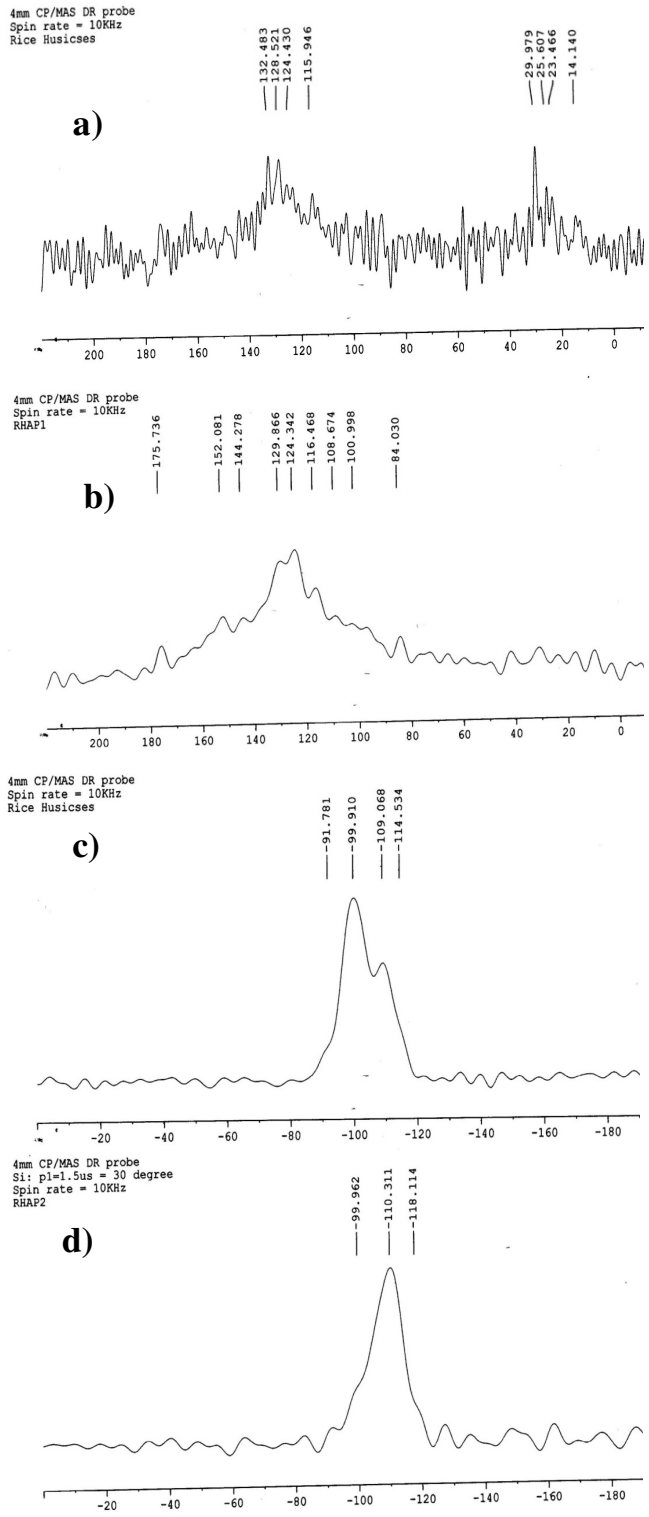

Figure 2. Solid state ^{13}C CP Mas spectra of a) RHA, b) PANI/RHA and ^{29}Si CP Mas spectra of c) RHA d) PANI/RHA.

Q^2 [geminal silanol, $(–SiO)_2Si(OH)_2$], Q^3 [single silanol, $(–SiO)_3–SiOH$] and Q^4 [siloxane, $(SiO)_4Si$] silicon atoms respectively.

The peaks obtained for PANI/RHA at -99 and -109 ppm (Figure. 2c) indicates the existence of Q^3 and Q^4 silicon atoms as similar to that of neat RHA. The disappearance of peak at -99 ppm is attributed to the some structural changes occurred in the Q^2 silicon atom (Figure. 2d) due to the interaction of RHA with polyaniline through weak Van der Waal's forces and hydrogen bonding. [29-34]

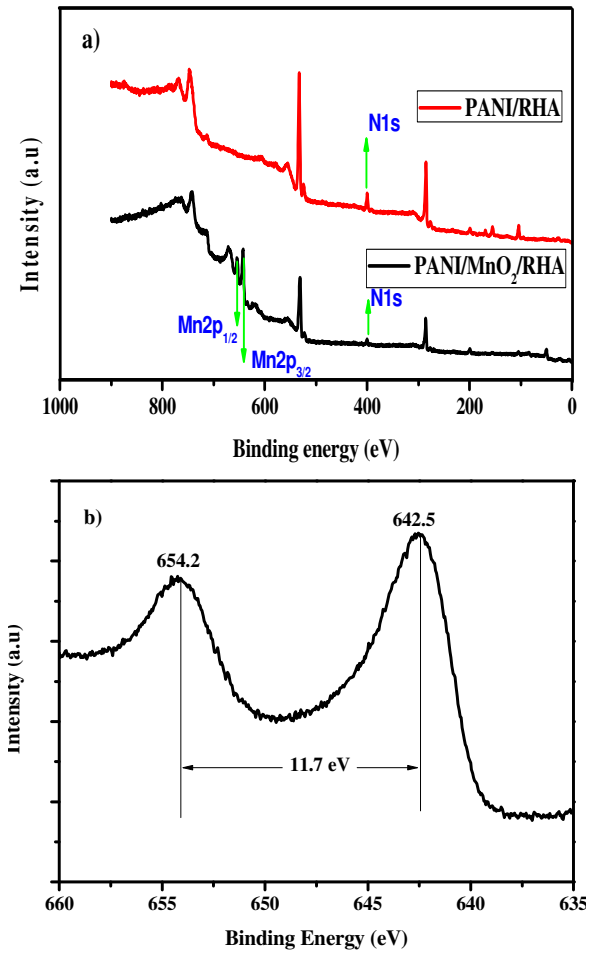

Figure 3. XPS Spectrum of a) PANI/RHA, PANI/MnO_2/RHA nanocomposites and b) manganese of PANI/MnO_2/RHA nanocomposites.

Further, the X-ray photoelectron survey spectrum presented in Figure 3a and it confirms the grafting of polyaniline through the presence of N atom at 400 eV in addition to the Si, C, and O atoms in PANI/RHA nanocomposites. Additionally the presence of Mn atom in the PANI/MnO_2/RHA nanocomposites was also ascertained from the peak existed at 642.2 eV and 653.9 eV.

Figure. 3b illustrates the existence of Mn 2p3/2 and Mn 2p1/2, whose binding energies were 642.2 eV and 653.9 eV. These binding energy values were confirming the presence of Mn^{4+} in the nanocomposites. Further the spin energy separation of 11.7 eV is also found to show good agreement with reported data of Mn 2p3/2 and Mn 2p1/2 in MnO_2. [28]

The thermal stability of the RHA, PANI/RHA and PANI/MnO_2/RHA was analyzed using thermo gravimetric analyzer and the thermograms are illustrated in Figure 4. Three major region of weight losses were observed in thermograms of RHA, PANI/RHA, PANI/MnO_2/RHA. The initial stage degradation was observed below 200 °C may be attributed to the water molecules from physically adsorbed on the surface of composites. Weight loss in the temperature range from 200–530 °C corresponds to the beginning of degradation of the polyaniline chain coated over the hybrid nanocomposites. [25] At above 530 °C indicates

the complete degradation of polyaniline and the evolution of oxygen from MnO_2. [35] Among the three composites, PANI/MnO_2/RHA were found to be more stable up to 530 °C, due to higher MnO_2 content.

Figure 5 shows that the N_2 adsorption and desorption isotherms of RHA, PANI/RHA and PANI/MnO_2/RHA. The rice husk ash shows 95 m^2g^{-1} surface areas with 0.20 cm^3g^{-1} pore volume. Amorphous carbon and silica formed during burning are key factors for the surface area of rice husk ash on burning at 350 °C. However, the fusion of particles at above 350 °C leads to partially closing of pores and resulted in crystalline silica's with lower surface area. [36, 37]

Similarly, the N_2 adsorption and desorption isotherms of PANI/RHA and PANI/MnO_2/RHA suggest the presence of mesopores nature in both nanocomposites with type IV hysteresis loops. However PANI/MnO_2/RHA shows 558.7 m^2g^{-1} surface areas with 0.08 cm^3g^{-1} pores volume whereas PANI/RHA endows only 163 m^2g^{-1} surface areas with 0.19 cm^3g^{-1} pore volumes. The increased surface area of PANI/MnO_2/RHA may be attributed to the decreased particle size of the nanocomposites and it is also reported that the presence of MnO_2 can offer higher surface area. Further, the tertiary composites constituted with MnO_2 and polyaniline contributes to the enhanced surface area of the developed nanocomposites than the pristine material. [38-42] Further, the highly amorphous nature of the nanocomposites (Figure 6.) also contributes to the enhancement of surface area.

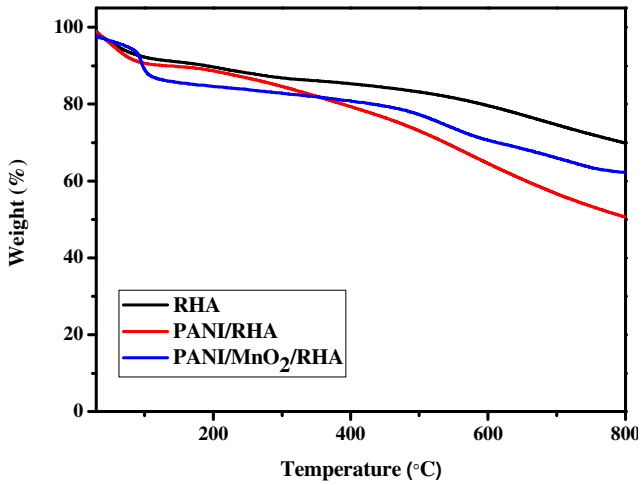

Figure 4. TGA Profile of RHA, PANI/RHA and PANI/MnO_2/RHA nanocomposites.

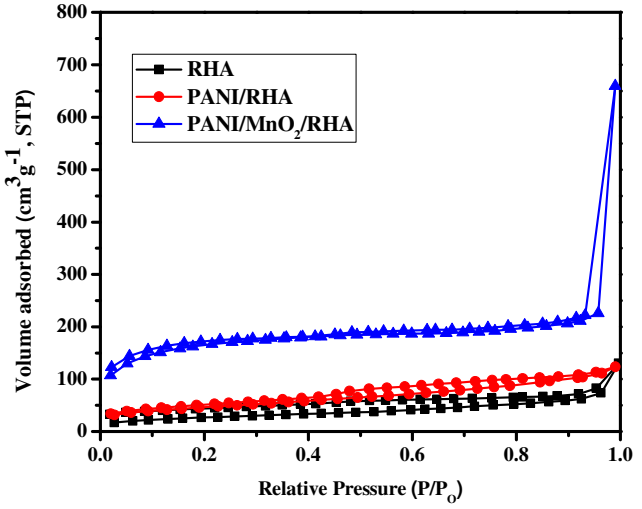

Figure 5. BET profile of a) RHA b) PANI/RHA and c) PANI/MnO_2/RHA nanocomposites.

The X-ray diffractogram of RHA, MnO_2, MnO_2/RHA, PANI/RHA and PANI/MnO_2/RHA are presented in the Figure 6. The broad reflection at 20° illustrates amorphous nature of RHA (Figure 6a). Similarly the MnO_2 doped RHA also shows a broad reflection at 20°.[43]

However, low intense and broad peaks appeared at 37.2° and 66.4° confirms the existence of MnO_2. The weak and broad signal of MnO_2 suggesting the amorphous nature and are similar with previous reports [44, 45]. The peaks appeared at 9.5° and 25° in Figure 6d confirms the polyaniline grafting in the PANI/RHA nanocomposites. The reflection of PANI at 25° with d-spacing (~3.5 Å) corresponds to the face-to-face interchain stacking distance between phenyl rings. [2, 46- 49] It is noteworthy that no distinct MnO_2 reflection was observed in the tertiary PANI/MnO_2/RHA composite indicating that that the surface of the MnO_2/RHA has been homogenously and densely grafted with polyaniline layer. Further it was reported that polymerization of PANI, will disturb the crystal structure of MnO_2 and thus led to the formation of amorphous MnO_2 [50-52]. Thus, the amorphous MnO_2 tunnel structures which should be convenient for cation diffusion. Subsequently, this can render a large capacitance [53].

The SEM micrographs of RHA, PANI/RHA, and PANI/MnO_2/RHA are illustrated in Figure 7a-c. The polyaniline grafting over the RHA is achieved by surface polymerization, which also seems to be uniform and shows the compatibility of rice husk ash with polyaniline. The adhesion of polyaniline was achieved in not only at macroscopic level, but also mesopores level of the rice husk. [54]

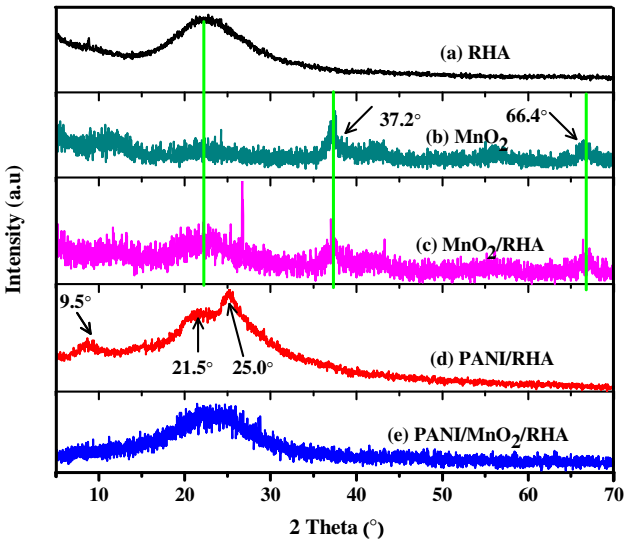

Figure 6. XRD Profile of a) RHA, b) MnO_2, c) MnO_2/RHA, d) PANI/RHA and PANI/MnO_2/RHA nanocomposites.

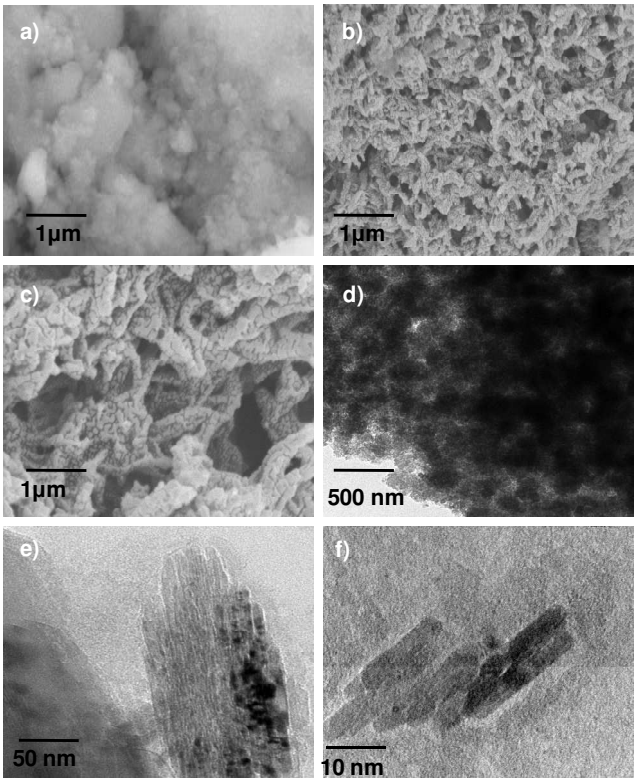

Figure 7. SEM micrograph of a. RHA, b. PANI/RHA and c. PANI/MnO_2/RHA nanocomposites and TEM micrograph of d. PANI/RHA and (e-f) PANI/MnO_2/RHA nanocomposites. Inset of Figure 7f is diffraction pattern of PANI/MnO_2/RHA.

Further, the fibrous like appearance of PANI offers higher surface area with improved porosity for both PANI/RHA and PANI/MnO_2/RHA nanocomposites. The same was supported by the N_2 adsorption studies, which affords high surface area of PANI/RHA (Figure 5).

It is also found that, the MnO_2 nanoparticles are successfully and uniformly deposited over the surface of the RHA like needle morphology, which are also indicated with arrow mark in the supporting information (Figure S5). [55] Thus, the –OH group present in the RHA network also acts as an anchor sites for Mn^{4+} ion. This phenomenon was well supported in Figure 7e and 7f, which affords homogeneous nucleation of MnO_2 in RHA and PANI grafting. [56] The composition of the PANI/RHA and PANI/MnO_2/RHA obtained from EDAX studies were presented in supporting information (Figure S2a and S2b) and Table S3

Figure 8a. Illustrates that the Cyclic Voltammograms (CV) of RHA, PANI/RHA and PANI/MnO_2/RHA at 30 mV scan rate in 0.5 M Na_2SO_4 electrolyte from -0.2 to 0.6 V potential window. The formation of rectangular curve without any redox behaviors, clearly illustrates that the neat RHA, PANI/RHA and PANI/MnO_2/RHA demonstrates the clear capacitance behavior. Among the nanocomposites, more Faradic current response was obtained with PANI/MnO_2/RHA. Due to the effective utilization of both doped MnO_2 with conductive PANI layer of PANI/MnO_2/RHA, larger increase in the Faradic performance with fast and reversible capacitance was achieved. Faradic behavior of neat rice husk ash may be attributed to the presence of 25 wt % carbon content of lignin in the rice husk ash, which was obtained from the thermal treatment of rice husk and supported by the EDAX study of RHA (supporting information Figure S1b and Table S3). However, PANI grafted RHA, exhibits higher current response with larger rectangular area due to the enhanced conductance of the PANI/RHA. This enhanced Faradic behavior of PANI/RHA may be attributed to the presence of PANI with fibrous morphology layer on the RHA surface, which offers high surface area and thus facilitates larger electrode/electrolyte interface area with enhanced electron transfer through the conductive network [2, 57]. Further, Figure 8b-d illustrates that the uniform rectangular shape even at higher scan rates, which suggest the characteristic behavior of double layer capacitance.

Further, evaluations of capacitance behavior with galvanostatic charge–discharge study at 0.5 – 5 mA/g are illustrated in Figure 9a-c for the composites of RHA, PANI/RHA and PANI/MnO_2/RHA. It is noteworthy that the PANI/MnO_2/RHA and PANI/RHA nanocomposite tends to show 135 F/g and 42.5 F/g specific capacitance respectively at a low current density of 0.5 mA/g.

The nanocomposites developed with PANI grafted and MnO_2 doped PANI grafted are found to show 17 and 54 fold higher capacitance than that of rice husk ash whose capacitance is 2.5 F/g. Large surface area with mesoporous morphology offered by MnO_2 and high conductive polyaniline network jointly provides better conducting pathways for both ionic (Na^+) and electronic (e^-) transportation during the rapid charge/discharge process and facilitates the high specific capacitance of PANI/MnO_2/RHA nanocomposites.[35, 57-59]

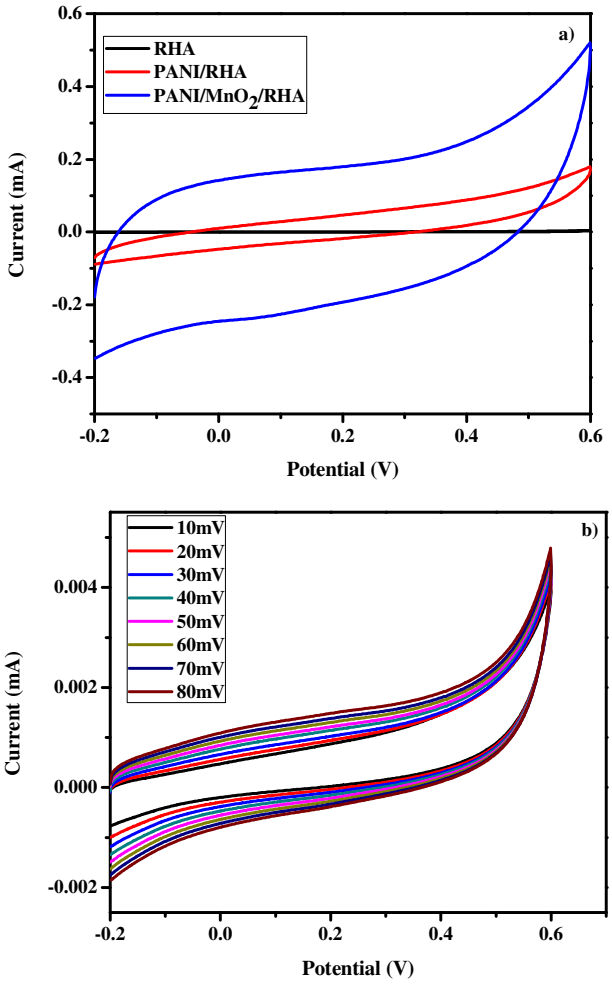

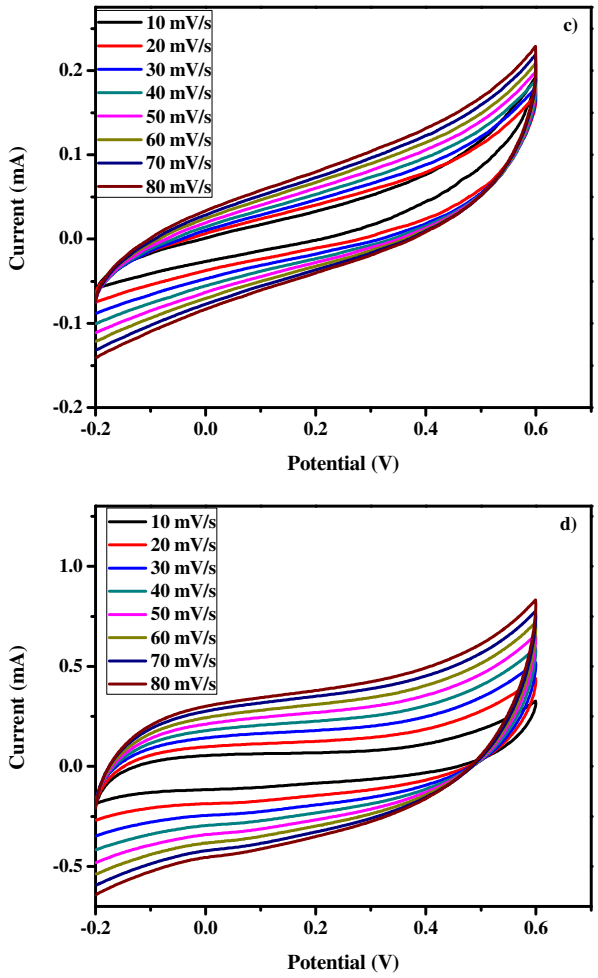

Figure 8a. Illustrates the Cyclic Voltammograms (CV) curves of RHA, PANI/RHA and PANI/MnO_2/RHA nanocomposites at 30 mV scan rate. Figure 8b-d Cyclic Voltammograms (CV) of RHA, PANI/RHA and PANI/MnO2/RHA nanocomposites at different scan rate in 0.5 M Na_2SO_4 electrolyte from -0.2 to 0.6 V potential windows.

Further, the carbon content present in the silica rich rice husk ash act as a binding material in addition to their Faradic behavior. Thus, it inhibits the addition of active materials like active carbon in electrode preparation. The resulting rate capabilities of the developed composites are compared in Figure 9d. For the PANI/MnO_2/RHA nanocomposites, the specific capacitance at the current density of 0.5, 0.7, 1.0,

and 3.0 mAg^{-1} was found to be 130, 89, 70, and 57 F/g respectively. However when the current rate was raised to 0.7, 1.0, and 3.0 mA/g the resulted capacitance retention was found as 70.6, 53.8, and 43.8 %, respectively. However, the RHA and PANI/RHA tends to show only 0.1% and 32.2 % retention, when the current density is raised to 3.0 mA/g from 0.5 mA/g respectively. Thus, the PANI/MnO_2/RHA sample retains maximum rate capability. The long-term cycling stability of the PANI/MnO_2/RHA and PANI/RHA nanocomposites are also studied by charge-discharge measurements at a current density of 0.5 mAg^{-1} for 1000 cycles and it was illustrated in the Figure 9e. The nanocomposites PANI/MnO_2/RHA exhibited a high electrochemical stability with 74.5% capacitance retention, whereas the PANI/RHA shows only 66.4 % retention. The improved cycling stability of PANI/MnO_2/RHA may be due to the large surface area with mesopores and presence of Si core of RHA with doped MnO_2 offers more stability solid skeleton to interlink polyaniline skeleton in turn, the grafted PANI protects the MnO_2 from dissolving in electrolyte. [2, 60, 61] The lowering capacitance of PANI/RHA is probably due to the degradation of polyaniline skeleton.

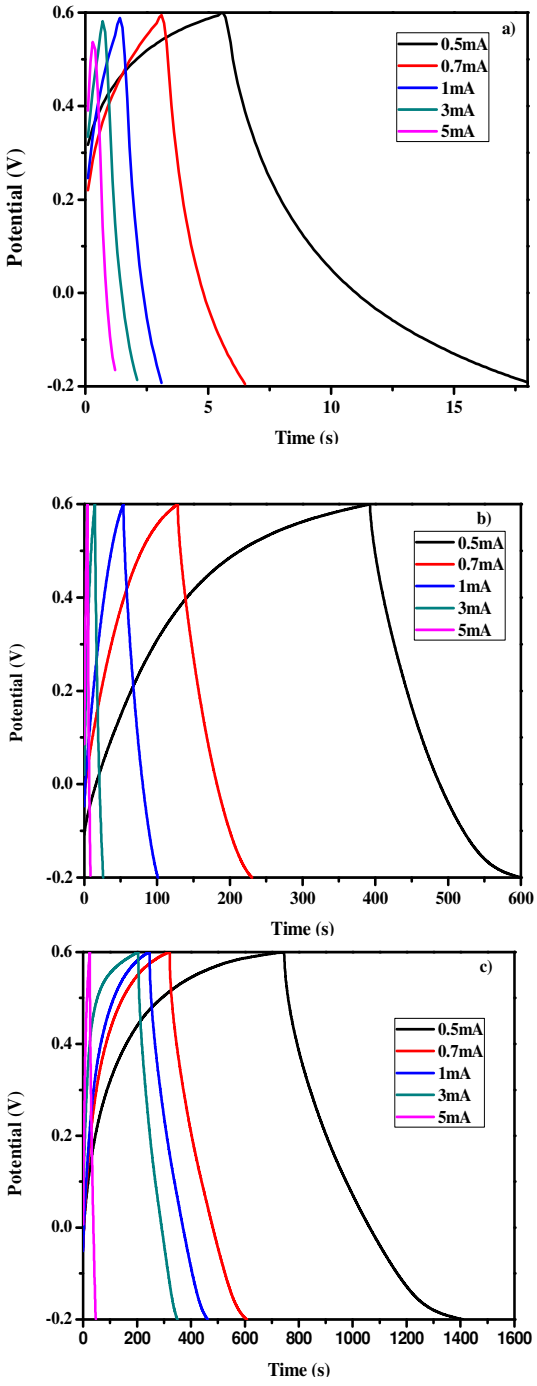

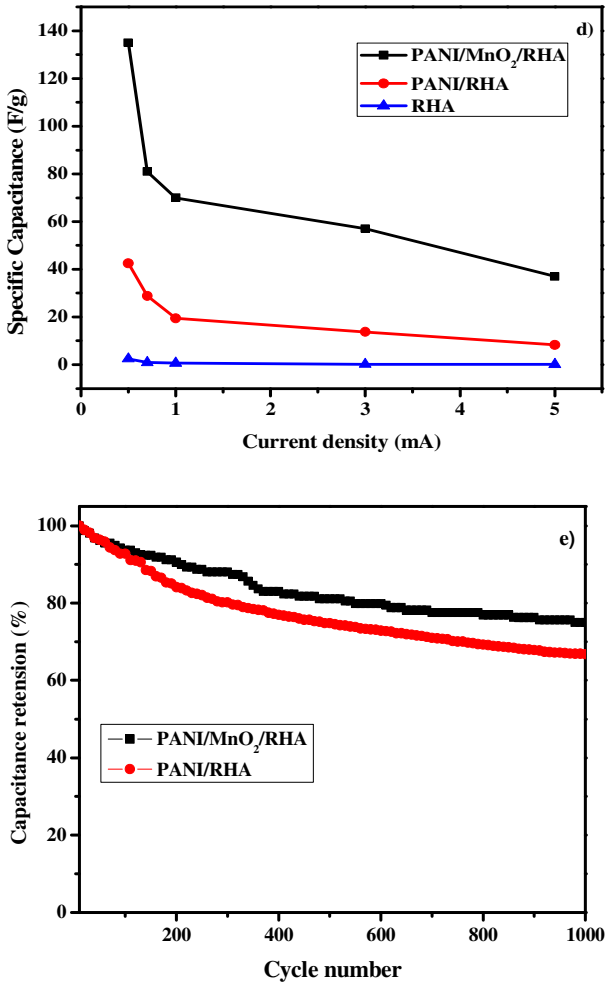

Figure 9. illustrates the Charging - Discharging curve of a) RHA, b) PANI/RHA and c) PANI/ MnO_2/RHA Charge-discharge at current densities of 0.5-3 mA g-1. (d) Specific capacitance as a function of different current densities of RHA, PANI/RHA and PANI/ MnO_2/RHA. e) Specific capacitance versus cycling number at 0.5 mA/g of the PANI/RHA and PANI/ MnO_2/RHA nanocomposites.

Electrochemical impedance spectra in the form of Nyquist plots of RHA, PANI/RHA and PANI/MnO_2/RHA are presented in Figure 10. The electrochemical behavior at the interface between the electrode and electrolyte was well understood from the semicircle in the high frequency region and a 45° capacitive slope in the low frequency region.

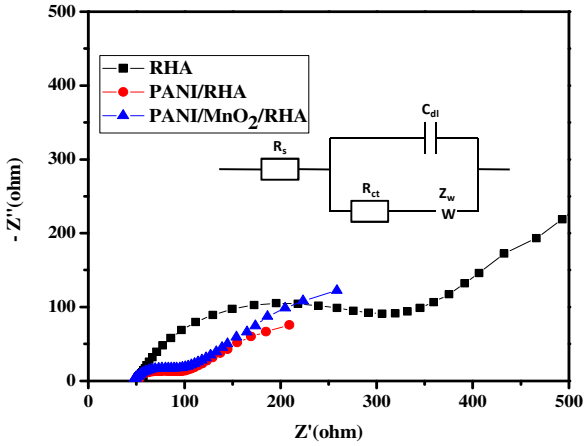

Figure 10. Nyquist Impedance spectra of RHA, PANI/RHA and PANI/MnO_2/RHA.

Table 1 Charge-transfer resistance of the different electrode and electrolyte interface

Electrode	R_e (ohm)	C_{dl} (F)	R_{ct} (ohm)	Z_w (ohm)
RHA	51.32	1.74 e-6	189.30	0.00065
PANI/RHA	56.74	1.00 e-6	36.32	0.00002
PANI/MnO_2/RHA	51.51	2.15 e-6	34.46	0.00004

Components include electrolyte resistance, intrinsic resistance of active material and contact resistant do the factors constitute the semicircle behavior. The charge-transfer resistances of the different electrodes and electrolytes interface are presented in Table 1. From the results of R_{ct}, the PANI/MnO_2/RHA system shows that the least charge transfer resistance among the three electrode materials. Due to the presence of capacitive materials and conductive network both in macro and mesoscopic levels of RHA the PANI/MnO_2/RHA nanocomposites delivered the larger Faradic response. [62, 63]

Conclusion

The renewable bio source of RHA was used over energy storage systems without any further chemical activation. The grafting of polyaniline over the rice husk ash surface was confirmed by ^{29}Si Cp-mas, XPS and EDAX. In addition, doping of MnO_2 was also confirmed by XPS survey. The electrochemical studies of PANI/MnO_2/RHA hybrid nanocomposite shows higher value of capacitance of 135 F/g along with superior stability and reversibility for long time. Thus, the renewable bio source RHA can be used in the form of an anode material for the fabrication of super capacitors, which can be utilized at large scale with competitive cost in future.

Acknowledgement

The authors thank BRNS, G. No: 2012/37C/9/BRNS, Mumbai, Govt. of India., for the financial support and also thank Dr. Manmohan Kumar, Senior Scientific Officer, BARC, Mumbai. The authors thank to Dr. M.R.Vengatesan, Sungkyunkwan University, Suwon, South Korea. Dr. S. Devaraju, Pusan National University, Busan, 609-735, South Korea, and Dr. Padmanaban, Dept. of Physics, Anna University for their support.

References

1. M. Biswal,. A. Banerjee, M. Deo,. and S. J. Ogale, Energy Environ. Sci., 2013, **6**, 1249.
2. M. Kim, S. Cho, J. Song, S. Son and J. Jang, Appl. Mater. Interfaces., 2012, **4**, 4603.
3. W.T. Deng, X.B. Ji, Q.Y. Chen and C.E. Banks, RSC Advances 2011, **1,** 1171.
4. C.D. Lokhande, D.P. Dubal and O.S. Joo, Curr. Appl Phys. 2011, **11** 255.
5. Z. Algharaibeh, X.R. Liu and P.G. Pickup, J. Power Sources 2009, **187**, 640.
6. Y.H. Lin, T.Y. Wei, H.C. Chien and S.Y. Lu, Adv. Energy Mater., 2011, **1,** 901.
7. H. Jiang, T. Zhao, C.Z. Li and J. Ma, J. Mater. Chem. 2011, **21**, 3818.
8. M. Hasan, M. Jamal and K.M. Razeeb, Electrochim. Acta., 2012, **60,** 193.
9. H. Shi, Electrochim. Acta. 1996, **41**, 1633.
10. D. Qu and H. Shi, J. Power Sources., 1998, **74**, 99.
11. Y. Guo, J. Qi, Y. Jiang, S. Yang, Z. Wang and H. Xu, Mater. Chem. Phys. 2003, **80**, 704.
12. N. Bagheri and J. Abedi, Chem. Eng. Res. Des. 2009, **87**, 1059.
13. M.T. Tsay and F.W. Chang, Applied Catalysis A: General., 2000, **203**, 15.
14. M. Ahmaruzzaman and V.K. Gupta, Ind. Eng. Chem. Res., 2011, **50**, 13589.
15. M.Y. Ahmad Fuad, Z. Ismail, M.S. Mansor, Z.A. Mohd Ishak and A.K. Mohd Omar, Polym. J., 1995, **27**, 1002.
16. Y. C. Y. Zhu, Z. Wang, Y. Li, L. Wang, L.Ding, X. Gao, Y.Ma, Y. Guo, Adv. Colloid Interface Sci., 2011, **163**, 39.
17. X. He, P. Ling, M.Yu, X. Wang, X. Zhang, M. Zheng, Electrochimic Acta., 2013, http://dx.doi.org/10.1016/j.electacta.2013.05.050
18 L. John Kennedy,J. Judith Vijaya, and G. Sekaran., Ind. Eng. Chem. Res. 2004, **43,** 1832.
19. N. Liu, K. Huo, M.T. McDowell, J. Zhao and Y. Cui, Sci. Rep., 2013, **3,** 1.
20. L. Wang, Z. Schneppb and M. M. Titirici, J. Mater. Chem. A., 2013, **1,** 5269.
21. S. Kumagai, M. Sato and D. Tashima, Electrochim. Acta., 2013, **114**, 617.
22. X. He, P. Ling, M. Yu, X. Wang, X. Zhang and M. Zheng, Electrochim. Acta, 2013, **105**, 635.
23. A. Imyim, E. Prapalimrungsi, J Hazard Mater., 2010, **184**, 775.
24. M. Ghorbani and H. Eisazadeh, Compos Part B-Eng., 2013, **45,** 1.
25. M. Ghorbani and H. Eisazadeh, Synt. Met., 2012,**162,** 527.
26. M. Ghorbani, M.S. Lashkenari and H. Eisazadeh, Synt. Met., 2011, **161**, 1430.
27. M Ghorbani, H Eisazadeh and A A Ghoreyshi, Iranica Journal of Energy & Environment 3 (2012) 83-88.
28. J. Han, L. Li, P. Fang and R. Guo, J. Phys. Chem. C., 2012, **116,** 15900.
29. J.C.C. Freitas, F.G. Emmerich, and T.J. Bonagamba, Chem. Mater., 2000, **12**, 711.

30. F. Adam, H. Osman, and K. M. Hello, J. Colloid Interface Sci., 2009, **331,** 143–147.
31. X. Zhang, N. Zhao, W. Wei and Y. Sun, Catalysis Today, 2006, **115**, 102.
32. Y.Z. Wang, Y.C. Hsu, R.R.Wu and H.M. Kao, Synt. Met., 2003, **132**, 151.
33. Z.D. Zujovic, M.G. Nikoladis, P.A. Kilmartin, J.T. Sejdic, R.P. Cooney and G.A. Bowmaker, Appl. Magn. Reson 2005, **28**, 123.
34. S. Kaplan, E.M. Conwell, A.F. Richter and A.G. MacDiarmid, J. Am. Chem. Soc. 1988, **110**, 7647.
35. K.S. Kim and S.J. Park, J. Solid State Electrochem. 2012, **16,** 2751.
36. A.J. Schwanke, C.W. Lopes and S.B.C. Pergher, Mater Sci App., 2013 **4,** 468.
37. S. Karthikeyan and G. Sekaran, Phys. Chem. Chem. Phys., 2014, **16**, 3924.
38. J.Kim, H.Ju, A.I. Inamdar, Y. Jo, J. Han, H.Kim and H. Im Energy., 2014, **70**, 473.
39. S.Hassan, M. Suzuki, S. Mori and A.A.El-Moneim, RSC Adv.,2014,**4**,20479
40. A. Sumboja, C. Y. Foo, J. Yan, C. Yan, R. K. Gupta and P.S. Lee, J. Mater. Chem., 2012, **22**, 23921
41. W. Ni, D. Wang, Z. Huang, J. Zhao, Guoeng Cui, Mater. Chem. Phys., **2010** 124, 1151.
42. Guangqiang Han, Yun Liu, Lingling Zhang, Erjun Kan, Shaopeng Zhang, Jian Tan, & Weihua Tang. Scientific Reports., 2014, **4**, 4824
43. A. Imyin and E. Prapalimrungsi, J. Hazard. Mater. 2010, **184**, 775.
44. Y. Hou, Y. Cheng, T. Hobson, and J. Liu. Nano Lett. 2010**, 10**, 2727.
45. S. J. Bao, B. L. He, Y. Y. Liang, W. J. Zhou, H. L. Li, *Mater. Sci. Eng., A* 2005, **397**, 305.
46. X. Yan, Z. Tai, J. Chen, and Q. Xue, Nanoscale, 2011, **3**, 212.
47. K.Zhang, L. L. Zhang, X. S. Zhao,and J. Wu, Chem. Mater. 2010, **22**, 1392.
48. K. Lee, S.Cho, S. H.Park, A. J. Heeger, C. W.Lee, S. H. Lee, Nature. 2006, **441**,65.
49. B. H.Lee, S. H. Park, H.Back, K. Lee, Adv. Funct. Mater.2011, **21**, 487.
50. B. Mu, W. Zhang, S. Shao and A. Wang, Phys. Chem.Chem.Phys.,2014, **16**,787
51. A. H. Gemeay, I. A. Mansour, R. G. El-Sharkawy, A.B. Zaki, Eur. Polym. J. 2005, **41,** 2575.
52. P. Tang, L.Han, and L. Zhang, ACS Appl. Mater. Interfaces., **6,** 2014,10506.
53. W. Zou, W. Wang, B.He, M.L. Sun, Y. sheng Yin, J. Power Sources., 2010, **195**, 7489.
54. M. Ghorbani, M.S. Lashkenari and H. Eisazadeh, Synt. Met., 2011 **161**,1430.
55. S.A. Iranagh, L Eskandarian and R Mohammadi, Synt. Met.,. 2013, **172**, 49.
56. D.R. Rolison, J.W. Long, J.C. Lytle, A.E. Fischer, C.P. Rhodes, T.M. McEvoy, M.E. Bourga and A.M. Lubers, Chemical. Soc. Rev., 2009, **38**, 226.
57. J. Xu, K. Wang, S. Z. Zu, B. H. Han, and Z. Wei, ACS Nano., 2010, **4,** 5019.
58. P. Lv, Y. Y. Feng, Y. Li and W. Feng, J. Power Sources., 2012, **220**, 160.
59. Y. Liu, D. Yan, R. Zhuo, S. Li, Z. Wu, J. Wang, P. Ren, P. Yan and Z. geng, J. Power Sources, 2013, **242**, 78.
60. H. Jiang, Y. Dai, Y. Hu, W. Chen, and C. Li, ACS Sustainable Chem. Eng ., 2014, **2,** 70.
61. J.G. Wang, Y.Yang, Z. Huang, F.Kang, Electrochimica Acta., 2014, **130**, 642.
62. L Chen, Z Song, G Liu, J Qiu, C Yu, J Qin, M Lin, F Tian, W Liu, J. Phys. Chem. Solids, 2013, **74**, 360.
63. P.A. Basnayaka, M.K. Ram, E.K. Stefanakos and Ashok Kumar, Electrochimica Acta 2013, **92**, 376.

MnO_2 Doped Polyaniline Grafted Rice Husk Ash Nanocomposites and their Electrochemical Capacitor Applications

P. Prabunathan, [1] K. Sethuraman [1], and M. Alagar [1] *

[1]*Polymer Composite Lab, Department of Chemical Engineering, Anna University, Chennai-600 025, India*

Graphical Abstract: